

SuperWIMP Gravitino Dark Matter from Slepton and Sneutrino Decays

Jonathan L. Feng,¹ Shufang Su,² and Fumihiro Takayama¹

¹*Department of Physics and Astronomy,
University of California, Irvine, CA 92697, USA*

²*Department of Physics, University of Arizona, Tucson, AZ 85721, USA*

Abstract

Dark matter may be composed of superWIMPs, superweakly-interacting massive particles produced in the late decays of other particles. We focus on the case of gravitinos produced in the late decays of sleptons or sneutrinos and assume they are produced in sufficient numbers to constitute all of non-baryonic dark matter. At leading order, these late decays are two-body and the accompanying energy is electromagnetic. For natural weak-scale parameters, these decays have been shown to satisfy bounds from Big Bang nucleosynthesis and the cosmic microwave background. However, sleptons and sneutrinos may also decay to three-body final states, producing hadronic energy, which is subject to even more stringent nucleosynthesis bounds. We determine the three-body branching fractions and the resulting hadronic energy release. We find that superWIMP gravitino dark matter is viable and determine the gravitino and slepton/sneutrino masses preferred by this solution to the dark matter problem. In passing, we note that hadronic constraints disfavor the possibility of superWIMPs produced by neutralino decays unless the neutralino is photino-like.

PACS numbers: 95.35.+d, 98.80.Cq, 26.35.+c, 98.80.Es

I. INTRODUCTION

SuperWIMPs, superweakly interacting massive particles produced in the late decays of weakly-interacting massive particles (WIMPs), are promising non-baryonic dark matter candidates [1, 2]. Well-motivated superWIMP candidates are the gravitino in supersymmetric models [1, 2, 3, 4, 5, 6] and the first excited graviton in universal extra dimension models [1, 7].

The supersymmetric possibility is realized naturally in supergravity with a gravitino lightest supersymmetric particle (LSP) and a slepton or sneutrino next-to-lightest supersymmetric particle (NLSP). (Throughout this paper, “slepton” denotes a charged slepton.) Both the gravitino and the NLSP have weak-scale masses. The NLSP freezes out as usual with a relic density near the observed value. However, after time $t \sim 10^4 - 10^8$ s, it decays through

$$\begin{aligned}\tilde{l} &\rightarrow l\tilde{G} \\ \tilde{\nu} &\rightarrow \nu\tilde{G} .\end{aligned}\tag{1}$$

The gravitino then inherits much of the relic density of the slepton or sneutrino [8], and its relic density is naturally of the right magnitude without the introduction of new scales. This is in contrast to other gravitino dark matter scenarios, where the gravitino is a thermal relic and the desired density is obtained by an appropriately chosen gravitino mass $m_{\tilde{G}} \sim \text{keV}$ [9], or the gravitino is produced during reheating [5, 10], where the desired dark matter density is obtained only for a fine-tuned reheat temperature $T_R \sim 10^{10}$ GeV.

The decays of Eq. (1) occur well after Big Bang nucleosynthesis (BBN). An immediate concern, therefore, is that they might destroy the successful light element abundance predictions of BBN. In fact, BBN is not the only worry — the Planckian spectrum of the cosmic microwave background (CMB), the diffuse photon background, and bounds on late time entropy production from the coincidence between BBN and CMB baryometry all impose significant constraints. As demonstrated in Refs. [1, 2], however, these constraints on the electromagnetic (EM) energy released in the decays of Eq. (1) exclude some of the weak scale parameter space, but leave much of it intact. Of course, at the border between the excluded and allowed regions, slight deviations from standard cosmological predictions are expected, providing possible signals in future observations. In fact, the existing anomaly in the ${}^7\text{Li}$ abundance prediction of standard BBN may already be interpreted as a signal of superWIMP dark matter [2]. Such signals are particularly welcome, since superWIMP dark matter is so weakly interacting that it is impossible to detect through conventional direct and indirect dark matter searches.

The previous work, however, neglected hadronic energy produced in WIMP decays. This was natural, as the WIMP decays of Eq. (1) contribute only to electromagnetic energy, as we will discuss below. However, the three-body decays

$$\begin{aligned}\tilde{l} &\rightarrow lZ\tilde{G} , \nu W\tilde{G} \\ \tilde{\nu} &\rightarrow \nu Z\tilde{G} , lW\tilde{G} ,\end{aligned}\tag{2}$$

produce hadronic energy when the Z or W decays hadronically. Hadronic energy release is very severely constrained by the observed primordial light element abundances [11, 12, 13, 14, 15], and so even subdominant hadronic decays could, in principle, provide stringent constraints. These three-body decays may be kinematically suppressed when

$m_{\tilde{l},\tilde{\nu}} - m_{\tilde{G}} < m_W, m_Z$, but even in this case, four-body decays, such as $\tilde{l} \rightarrow l\gamma^*\tilde{G} \rightarrow lq\bar{q}\tilde{G}$, contribute to hadronic cascades and may be important. In this paper, we determine the hadronic branching fractions and compare them to BBN constraints on hadronic energy release. Although we focus on the supersymmetric case, our results may be extended straightforwardly with minor numerical modifications to the case of graviton superWIMPs in extra dimensions.

In evaluating the constraints, there are two possible approaches. As the superWIMP relic abundance is automatically in the right range, a natural assumption is that superWIMP gravitinos make up all of the non-baryonic dark matter, with

$$\Omega_{\text{SWIMP}} \simeq 0.23 . \quad (3)$$

This is the approach taken here. Note that Ω_{SWIMP} need not be identical to $\Omega_{\tilde{G}}$ — not all relic gravitinos need be produced by NLSP decays. Our assumption therefore requires that the other sources of gravitinos be insignificant. For the supersymmetric case, this typically implies an upper bound on reheat temperatures of $T_R \lesssim 10^{10}$ GeV [5, 10]. Higher reheat temperatures may also be allowed [16, 17] and are desirable, for example, to accommodate leptogenesis. For the universal extra dimension case, the requirement of insignificant Kaluza-Klein graviton production during reheating implies $T_R \lesssim 1$ to 10^2 TeV, depending, in part, on the number of extra dimensions [7].

On the other hand, the Universe has proven to be remarkably baroque, and there is no guarantee that dark matter is composed of only one component. One might therefore relax the constraint of Eq. (3) on the superWIMP energy density and assume, for example, that the NLSP freezes out with its thermal relic density $\Omega_{\text{NLSP}}^{\text{th}}$. The superWIMP gravitino density is then $\Omega_{\text{SWIMP}} = (m_{\tilde{G}}/m_{\text{NLSP}})\Omega_{\text{NLSP}}^{\text{th}}$. In this approach, the gravitino density may be low and even insignificant cosmologically. From a particle physics viewpoint, however, the viability of the gravitino LSP scenario is still worth investigation, as it has strong implications for the superpartner spectrum and collider signatures, independent of its cosmological importance.

These approaches differ significantly, not only in the viewpoint taken, but also in their implications. Suppose, for example, that the gravitino and NLSP masses are both parametrized by a mass scale m_{SUSY} . The NLSP number density then scales as $1/m_{\text{SUSY}}$ if one assumes Eq. (3), but scales as m_{SUSY} if one assumes a thermal relic NLSP density, since $\Omega_{\text{NLSP}}^{\text{th}} \propto \langle\sigma v\rangle^{-1} \propto m_{\text{SUSY}}^2$, where $\langle\sigma v\rangle$ is the thermally-averaged NLSP annihilation cross section. Low masses are excluded in the former case, while high masses are disfavored in the latter. We consider both approaches to be worthwhile, but defer discussion of the thermal relic density approach, along with its very different consequences for the superpartner spectrum and implications for collider physics, to a separate study [18].

Assuming a fixed Ω_{SWIMP} here, we find that gravitino superWIMPs provide a viable solution to the dark matter problem. We determine the allowed masses for the NLSP and gravitino. At the same time, we find that the hadronic energy constraint is significant and does in fact provide the leading constraint in natural regions of parameter space. We conclude that the analysis below must be done in any scenario with similar late decays. Given any standard cosmology, a significant thermal relic abundance of NLSPs will be generated, these NLSPs will eventually decay to superWIMPs, and the hadronic constraints we discuss below must be analyzed before the scenario may be considered viable.

In passing, we note that another possibility is that the NLSP is the lightest neutralino. For a general neutralino, the decays $\chi \rightarrow Z\tilde{G}, h\tilde{G}$ produce large hadronic energy release. These two-body modes are absent for photino-like neutralinos, where the only two-body

decay is $\tilde{\gamma} \rightarrow \gamma\tilde{G}$. However, even in this case, one cannot avoid hadronic activity from decay through a virtual photon, $\tilde{\gamma} \rightarrow \gamma^*\tilde{G} \rightarrow q\bar{q}\tilde{G}$, with a branching fraction of $\mathcal{O}(10^{-2})$. Given the stringency of constraints on hadronic energy release, the neutralino NLSP case is highly constrained. Assuming that Ω_{SWIMP} makes up a significant fraction of the dark matter, natural regions of parameter space are excluded [18]. In the current paper, we therefore focus on the more promising possibilities of slepton and sneutrino NLSPs.

The paper is organized as follows. In Sec. II, we summarize what is known about constraints on EM and hadronic energy release in the early Universe. In Sec. III, we give a detailed description of the gravitino superWIMP scenario with a slepton or sneutrino NLSP. In Sec. IV, we determine the hadronic energy release from slepton and sneutrino decays and find the allowed mass regions. We summarize in Sec. V. The relevant gravitino interactions, decay amplitudes, and three-body hadronic decay width formulae are collected in the Appendix.

II. LATE TIME ENERGY INJECTION AND BBN

The overall success of standard BBN places severe constraints on energy produced by particles decaying after BBN. Given the baryon density specified by CMB measurements [19], the prediction of standard BBN [20] for deuterium agrees well with observations [21]. This concordance is less perfect, but still reasonable, for ^4He [22, 23]. On the other hand, current observations of ^7Li [24, 25, 26] are consistently lower than predictions; this is the leading anomaly in light element abundances at present. The abundances of ^3He and ^6Li also provide constraints, although these are subject to more theoretical uncertainties as discussed below.

In this section, we review the constraints from these element abundances on energy release in the early Universe. Although a unified analysis is necessary for detailed conclusions, we review the constraints on EM and hadronic energy release in turn. A schematic summary of the discussion in this section is given in Fig. 1.

The constraints on EM energy release are well understood, and we begin with a brief summary of the results. (For details, see Ref. [27].) High energy photons and leptons produced by late-decaying particles are quickly thermalized through interactions with background (BG) particles. High energy photons, for example, initiate EM cascades through processes like $\gamma\gamma_{\text{BG}} \rightarrow e^+e^-$ and $\gamma e_{\text{BG}} \rightarrow \gamma e$, and the initial energy is quickly converted to very soft photons. The same is true for high energy electrons and muons. High energy taus decay to mesons, but these decay and produce EM cascades before interacting hadronically. (See Ref. [2] and the analysis below.) Injected leptons of all three families therefore contribute dominantly to EM energy and negligibly to hadronic energy.

The energy distribution of the resulting photons is highly suppressed for $E_\gamma > E_{\text{max}}$, where

$$E_{\text{max}} = \frac{m_e^2}{22T} \simeq 12 \text{ MeV} \left[\frac{\text{keV}}{T} \right] \quad (4)$$

is related to the energy threshold for $\gamma\gamma_{\text{BG}} \rightarrow e^+e^-$ [28]. Here T is the BG photon temperature; in the radiation-dominated era, it is related to time by

$$t \simeq 1.0 \times 10^6 \text{ s} \left[\frac{\text{keV}}{T} \right]^2. \quad (5)$$

Time	(sec)	1	10	10 ²	10 ³	10 ⁴	10 ⁵	10 ⁶	10 ⁷
Hadronic Energy	Thermalizes through EM interactions				Interacts with background hadrons				
	$p + e \leftrightarrow n + \nu$ No constraints	$n + p \rightarrow D \rightarrow {}^4\text{He}$ ⁴ He overproduction		$n + p \rightarrow D$		$n + {}^4\text{He} \rightarrow D$ D overproduction			
EM Energy	Thermalizes through EM interactions								
	Constraints weak					$\gamma + D \rightarrow n + p$ D overdestruction		$\gamma + {}^4\text{He} \rightarrow D + D$ D overproduction	
Overall	No constraints	⁴ He overproduction		D overproduction		Possible EM/had cancellation		D overproduction	

FIG. 1: Summary of the leading constraints from D and ⁴He on late time EM and hadronic energy injection into the early Universe. Constraints from ³He and ⁶Li may also be important. (See text.)

Because of this rapid thermalization, constraints on EM energy depend on the total amount of energy released and are essentially independent of the shape of the initial energy spectrum.

For $t \lesssim 10^4$ s, the BBN constraints are rather weak since E_{max} is too small to destroy any light elements. For $10^4 \text{ s} \lesssim t \lesssim 10^6$ s, the Universe is hot and E_{max} is low, and so only light elements with very low binding energies can be destroyed. The main constraint is from the overdestruction of D, with a binding energy of only 2.2 MeV. For $t \gtrsim 10^7$ s, the Universe is cooler and E_{max} becomes high enough that ⁴He, with binding energy 19.8 MeV, is destroyed. Even a small amount of ⁴He photo-dissociation becomes a significant production mechanism for ³He and D, since the observed abundances of ³He and D are much lower than that of ⁴He. The main constraint is from the overproduction of D.

Between 10^6 s and 10^7 s there is a region where the overdestruction and overproduction of D cancel. For sufficiently high energy release in this region, the D abundance is that of standard BBN, but ⁷Li, with binding energy 2.5 MeV, is destroyed through ${}^7\text{Li} + \gamma \rightarrow n + {}^6\text{Li}$. The observed ⁷Li abundance [24, 25, 26] is in fact low compared to the predictions of standard BBN [20]. We see, then, that the ⁷Li abundance can be brought into agreement with observations without upsetting the D concordance for decay times in this window. For $\eta = n_B/n_\gamma = 6.0 \times 10^{-10}$, the best fit values are [27]

$$\xi_{\text{EM}} \approx 10^{-9} \text{ GeV} , \quad t \approx 3 \times 10^6 \text{ s} , \quad (6)$$

where

$$\xi_{\text{EM}} \equiv \epsilon_{\text{EM}} B_{\text{EM}} Y_{\text{NLSP}} \quad (7)$$

is the emitted EM energy density. Here ϵ_{EM} is the initial EM energy released in NLSP decay, and B_{EM} is the branching fraction of NLSP decay into EM components. $Y_{\text{NLSP}} \equiv n_{\text{NLSP}}/n_\gamma$

is the NLSP number density just before NLSP decay, normalized to the BG photon number density $n_\gamma = 2\zeta(3)T^3/\pi^2$. It can be expressed in terms of the superWIMP abundance:

$$Y_{\text{NLSP}} \simeq 3.0 \times 10^{-12} \left[\frac{\text{TeV}}{m_{\text{SWIMP}}} \right] \left[\frac{\Omega_{\text{SWIMP}}}{0.23} \right]. \quad (8)$$

The parameters of Eq. (6) are naturally realized in the superWIMP scenario when a weak-scale NLSP decays to a weak-scale superWIMP with the observed dark matter density [2].

The numerical constraints on EM energy release as a function of the particle decay lifetime have been determined in Ref. [27], using the following criteria:

$$\text{D low : } D/H < 1.3 \times 10^{-5} \quad (9)$$

$$\text{D high : } D/H > 5.3 \times 10^{-5} \quad (10)$$

$${}^4\text{He low : } Y_p < 0.227 \quad (11)$$

$${}^7\text{Li low : } {}^7\text{Li}/H < 0.9 \times 10^{-10}. \quad (12)$$

We adopt these constraints in our consideration of EM energy release bounds.

Hadronic energy release, and its effects on BBN, has also been considered [11, 12, 13, 14, 15]. Although we are most interested in energy release at times $t \gtrsim 10^4$ s, we summarize here what is known for $t \gtrsim 1$ s for completeness.

As we will show below, for the decay times of interest, mesons decay quickly and so contribute to EM energy. Only protons and neutrons are sufficiently long-lived that they might be able to interact hadronically. For times $t \lesssim 150$ s, however, even high energy protons and neutrons (with energies $\gtrsim 100$ GeV) interact through EM scattering with BG photons before interacting with BG baryons. Injected high energy baryons then quickly become slow baryons, with the initial energy dissipated to EM energy. For such early times, this EM energy is harmless, as discussed above. Constraints are therefore functions of the number density of injected baryons $B_{\text{had}}Y_{\text{NLSP}}$, and independent of the initial baryon energy ϵ_{had} .

Slow baryons modify the number of neutrons and protons and therefore BBN predictions. In the very earliest era with $t \lesssim 1$ s, however, the weak interaction $p + e \leftrightarrow n + \nu$ is efficient, and so any deviation in the n/p ratio is washed out, and there are no strong bounds. For $t \gtrsim 1$ s, the weak interactions decouple. Slow baryons produced in late decays cause the n/p ratio to deviate from the standard BBN value. In particular, extra neutrons create D. For $1 \text{ s} \lesssim t \lesssim 100 \text{ s}$, the resulting D is immediately burned to form ${}^4\text{He}$, and so the dominant constraint is from overproduction of ${}^4\text{He}$. This constraint is weak since the ${}^4\text{He}$ abundance of standard BBN is already large. For $t > 100$ s, D can no longer burn into ${}^4\text{He}$ [11, 12] and the dominant constraint comes from D overproduction. This bound is significantly stronger, since the D/H ratio is $\sim 10^{-5}$.

At times $t \gtrsim 150$ s, injected baryons interact with BG baryons before thermalizing. These interactions create secondary hadrons that can modify BBN predictions. In this era, constraints depend in principle on both ϵ_{had} and $B_{\text{had}}Y_{\text{NLSP}}$ separately. In principle, the constraints do not simply depend on the product, because the total number of secondary hadrons created by an injected hadron is not always proportional to the injected hadronic energy. The dominant constraint is from secondary baryons destroying ${}^4\text{He}$ to overproduce D.

Quantitative analyses on the BBN constraints of the hadronic energy injection have been performed in Refs. [11, 12, 13, 14, 15]. As discussed above, formally, the constraints depend

on the lifetime τ of the decaying particle and on ϵ_{had} and $B_{\text{had}}Y_{\text{NLSP}}$ separately. However, the most recent analysis [15] finds that for decay times $\tau \lesssim 10^6$ s, when the hadronic constraint is most important, the constraints depend on the product $\epsilon_{\text{had}}B_{\text{had}}Y_{\text{NLSP}}$ to within a factor of 2 for $100 \text{ GeV} \leq \epsilon_{\text{had}} \leq 1 \text{ TeV}$ [29]. We will therefore assume this behavior and apply the hadronic constraint to times $\tau \lesssim 10^6$ s, where it is stronger than the EM constraint in the superWIMP scenario.

The authors of Ref. [15] assume the following constraints on the light element abundances (95% CL):

$$\text{D/H} = (2.8 \pm 0.8) \times 10^{-5} \quad (13)$$

$$Y_p = 0.238 \pm 0.004 \pm 0.010 \quad (14)$$

$$\log_{10}({}^7\text{Li/H}) = -9.66 \pm 0.112 \pm 0.6 . \quad (15)$$

In our analysis of hadronic energy injection, we take the constraints of Ref. [15] derived using these bounds and $B_{\text{had}} = 1$.

Note that the constraints of Eqs. (13)-(15) adopted for the hadronic energy analysis are less conservative than the constraints of Eqs. (9)-(12) used in the EM analysis of Ref. [27]. In particular, a significantly more aggressive D bound is assumed in the hadronic analysis. There is now impressive concordance between the baryon number determinations from D and CMB measurements, which further supports the narrow range of D/H given in Eq. (13). At the same time, existing anomalies in standard BBN may be indications that systematic errors are underestimated or that there is new physics, which would likely distort the D abundance, since D is very weakly bound.

There are several further comments to make. First, we have been treating the EM and hadronic effects separately. Of course, these effects can add constructively or destructively [14]. We have explained above that the dominant hadronic constraint for $t \gtrsim 10^4$ s is from D overproduction, whereas for the EM constraint it is from D overproduction for $t \gtrsim 10^6$ s and from D overdestruction for $10^4 \text{ s} \lesssim t \lesssim 10^6 \text{ s}$. For phenomena contributing to both EM and hadronic energy, then, the effects add constructively for $t \gtrsim 10^6$ s, but may cancel for $10^4 \text{ s} \lesssim t \lesssim 10^6 \text{ s}$, and there may be fingers of allowed region in the latter time interval.

Finally, although we consider only the constraints above on D/H, Y_p and ${}^7\text{Li/H}$, in Ref. [15], constraints from ${}^3\text{He/D}$ and ${}^6\text{Li/H}$ are also analyzed for late time EM and hadronic injections. These two abundances, however, are subject to more uncertainties. ${}^3\text{He/D}$ is considered because the destruction of ${}^4\text{He}$ could produce ${}^3\text{He}$ more easily than D, while the binding energy of ${}^3\text{He}$ is higher than that of D. However, the interpretation of ${}^3\text{He}$ measurements [30] may be subject to ambiguities arising from stellar production and destruction [31]. The ratio of ${}^6\text{Li}/{}^7\text{Li}$ has been observed in low metallicity halo stars and might also constrain late decays. The implications for EM cascades have also been explored in Refs. [32, 33]. Again, however, there are arguably significant systematic uncertainties arising from the higher depletion of ${}^6\text{Li}$ relative to ${}^7\text{Li}$ as a result of its smaller binding energy [34]. A better understanding of the connection between the primordial and observed abundances of ${}^6\text{Li}$ and ${}^7\text{Li}$ could provide a very powerful constraint on late decaying particles [35].

III. SLEPTON AND SNEUTRINO NLSP DECAYS

In the superWIMP dark matter scenario, superWIMPs have no effect on the early thermal history of the Universe. They are produced only through metastable NLSP decays, NLSP \rightarrow

\tilde{G} + SM particle, giving a gravitino relic density of

$$\Omega_{\text{SWIMP}} = \frac{m_{\tilde{G}}}{m_{\text{NLSP}}} \Omega_{\text{NLSP}}^{\text{th}} . \quad (16)$$

$\Omega_{\text{NLSP}}^{\text{th}} > 0.23$ is allowed, since $m_{\tilde{G}}/m_{\text{NLSP}} < 1$. The SM particles produced in the NLSP decay induce EM or hadronic cascades, which will affect the primordial abundance of light elements, as discussed in Sec. II.

The dominant decay mode for slepton NLSPs is $\tilde{l} \rightarrow l\tilde{G}$. Most of the energy released from the decay is transferred to EM cascades. The total energy released in slepton decay is

$$E_{\text{total}} = \frac{m_{\text{NLSP}}^2 - m_{\tilde{G}}^2}{2m_{\text{NLSP}}} . \quad (17)$$

The total injected EM energy density is, for $\Delta m = m_{\tilde{l}} - m_{\tilde{G}} \lesssim m_{\tilde{l}}$,

$$\xi_{\text{EM}} \equiv \epsilon_{\text{EM}} B_{\text{EM}} Y_{\tilde{l}} \sim \mathcal{O}(10^{-9} \text{ GeV}) \left[\frac{\epsilon_{\text{EM}} B_{\text{EM}}}{E_{\text{total}}} \right] \left[\frac{\Delta m}{300 \text{ GeV}} \right] \left[\frac{\text{TeV}}{m_{\tilde{G}}} \right] \left[\frac{\Omega_{\text{SWIMP}}}{0.23} \right] , \quad (18)$$

where $\epsilon_{\text{EM}} B_{\text{EM}}$ depends on the slepton's flavor, and Eq. (8) has been used. For selectrons and smuons, energetic electrons and muons quickly thermalize with the background photons. All the visible energy is transferred to the resulting EM cascade: $\epsilon_{\text{EM}} = E_{\text{total}}$, $B_{\text{EM}} = 1$. In the case of staus, the decays of taus could also produce mesons and neutrinos, in addition to electrons and muons. The EM activity depends on the lifetime and energy distribution of decay products. As estimated in Ref. [2], the EM energy released in stau decay is in the range $0.3E_{\text{total}}$ to E_{total} .

For the sneutrino NLSP case, the sneutrino mainly decays into neutrino and gravitino. The emitted high energy neutrino interacts with BG neutrinos and loses energy. If the neutrinos annihilate through $\nu\nu_{\text{BG}} \rightarrow e^+e^-$, an EM cascade is initiated. However, the annihilation takes place through weak interactions, and so its cross section may be small. The effect of the expansion of the Universe must also be taken into account [36, 37]. Sneutrino decays induce far less EM energy release than sleptons, but for decay times $\tau \lesssim 10^7$ s, there may still be some impact on BBN. For such decay times, however, much of the parameter space is excluded by considerations of hadronic BBN constraints, which will be discussed below. In what is left of this region, the gravitino mass is $m_{\tilde{G}} < \mathcal{O}(10)$ GeV. Such light gravitinos are less motivated in supergravity and so we have not considered this scenario in great detail here.

The decay width of the slepton into LSP gravitino is

$$\Gamma(\tilde{l}_{L,R} \rightarrow l_{L,R}\tilde{G}) = \frac{1}{96\pi M_4^2} \frac{m_{\tilde{l}}^5}{m_{\tilde{G}}^2} \left[1 - \frac{m_{\tilde{G}}^2}{m_{\tilde{l}}^2} \right]^4 , \quad (19)$$

where $M_4 = (16\pi G_N)^{-1/2}$. For $m_{\tilde{G}}/m_{\tilde{l}} \approx 1$, the slepton decay lifetime is

$$\tau(\tilde{l}_{L,R} \rightarrow l_{L,R}\tilde{G}) \simeq 3.6 \times 10^8 \text{ s} \left[\frac{100 \text{ GeV}}{\Delta m} \right]^4 \left[\frac{m_{\tilde{G}}}{\text{TeV}} \right] . \quad (20)$$

This expression is valid only when the gravitino and slepton are nearly degenerate, but we present it here as a useful guide for the reader. In the analysis below, we always use Eq. (19)

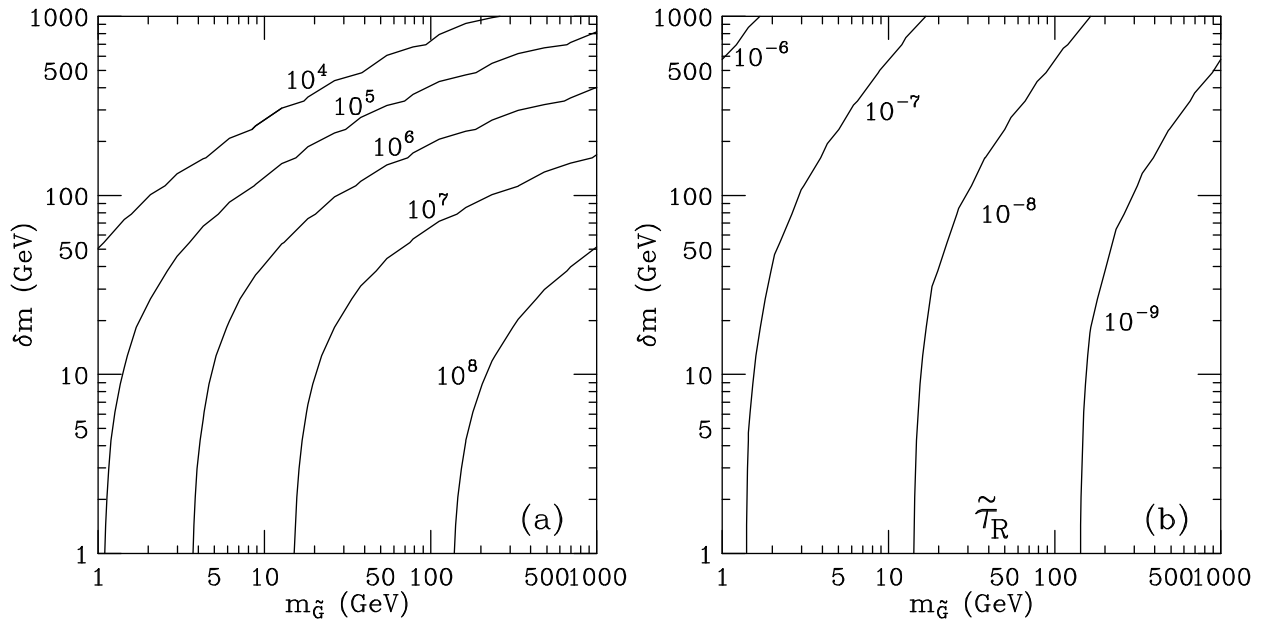


FIG. 2: (a) Lifetime (in seconds) for $\tilde{l}_{L,R}$, $\tilde{\nu}$ NLSPs and (b) EM energy release (in GeV) for the $\tilde{\tau}_R$ NLSP as functions of gravitino mass $m_{\tilde{G}}$ and mass difference $\delta m = m_{\tilde{l}} - m_{\tilde{G}} - m_Z$. For (b), we take $\epsilon_{EM} = 0.5E_{\text{total}}$, $B_{EM} = 1$, and $\Omega_{\text{SWIMP}} = 0.23$.

for the evaluation of the slepton decay lifetime. The slepton lifetime is given in Fig. 2a in the $(m_{\tilde{G}}, \delta m)$ plane, where

$$\delta m \equiv \Delta m - m_Z = m_{\tilde{l}} - m_{\tilde{G}} - m_Z . \quad (21)$$

Note that in the definition of δm , an additional m_Z is subtracted from Δm ; three-body decays, to be discussed below, are therefore always kinematically possible for $\delta m > 0$. The typical decay time is $10^4 \text{ s} \lesssim \tau \lesssim 10^8 \text{ s}$. For such decay times, there are strong constraints from the primordial abundance of the light element, as discussed earlier.

Contours of EM energy release $\xi_{EM} = \epsilon_{EM} B_{EM} Y_{\tilde{l}}$ are given in Fig. 2b for $\tilde{\tau}_R$ NLSPs, assuming $\epsilon_{EM} = 0.5E_{\text{total}}$, $B_{EM} = 1$, and $\Omega_{\text{SWIMP}} = 0.23$. We see that the EM energy release varies from $10^{-6} - 10^{-9}$ GeV and is largest for large δm and small $m_{\tilde{G}}$, when the decay lifetime is the shortest. The BBN constraints, however, are much weaker for early decays. As discussed in Ref. [2], considering EM energy constraints only, one finds that for a stau NLSP, $m_{\tilde{G}} \sim 300 - 500$ GeV and $\delta m \sim 200 - 1000$ GeV are allowed. Moreover, late time EM energy release from stau decays to gravitinos may resolve the current discrepancy in the ${}^7\text{Li}$ for $(m_{\tilde{G}}, \delta m) \approx (450 \text{ GeV}, 200 \text{ GeV})$. For selectron or smuon NLSPs, the EM constraints are slightly stronger since all the released decay energy is transferred to EM cascades.

The EM BBN constraints may be weakened by a number of possibilities. First, for decays in the range $10^4 \text{ s} \lesssim \tau \lesssim 10^6 \text{ s}$, the EM constraints may be weakened by cancellation between the effects of EM and hadronic energy release, as discussed above. Second, if not all of non-baryonic dark matter is superWIMPs, $\Omega_{\text{SWIMP}} < 0.23$, the contour lines for ξ_{EM} will shift toward the left, since $\xi_{EM} \propto \Omega_{\text{SWIMP}}$, and the allowed parameter space will be enlarged. Finally, if the NLSP is not a slepton but a sneutrino, the EM BBN constraints are, of course, much weaker, as the two-body decays contribute much less visible energy than in the slepton NLSP case.

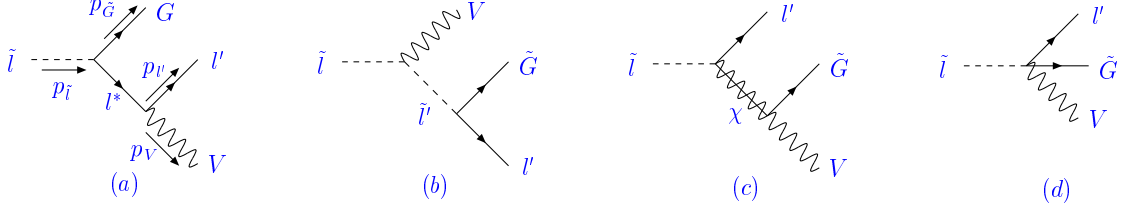


FIG. 3: Feynman diagrams for slepton decays $\tilde{l} \rightarrow l'V\tilde{G}$ leading to hadronic energy. χ in diagram (c) is a neutralino or chargino. When kinematically accessible, V is a Z or W boson. For small $\Delta m < m_Z, m_W$, the leading hadronic decay is $\tilde{l} \rightarrow l\gamma^*\tilde{G}$, followed by $\gamma^* \rightarrow q\bar{q}$.

IV. CONSTRAINTS FROM HADRONIC ENERGY RELEASE

As discussed in Sec. II, the abundances of light elements constrain the amount of hadronic energy injection into the early Universe. Although, for leptonic NLSPs, the hadronic energy release is much smaller than the EM energy release, the constraints on the hadronic energy release are much stronger. It is therefore important to evaluate in detail the hadronic activity induced by slepton and sneutrino NLSP decays.

Let us first study the slepton NLSP possibility. The main decay mode of sleptons is $\tilde{l} \rightarrow l\tilde{G}$. For selectron and smuon NLSPs, such decays induce only EM cascades. For stau NLSPs, however, the resulting tau lepton may decay into mesons, and these might interact with background hadrons and induce dangerous hadronic cascades. The interaction time of the produced mesons is

$$\begin{aligned} \tau_{\text{strong-int}} &= [\langle\sigma_{\text{had}}v\rangle n_B]^{-1} \simeq 18 \text{ s} \left[\frac{100 \text{ mb}}{\langle\sigma_{\text{had}}v\rangle} \right] \left[\frac{6 \times 10^{-10}}{\eta} \right] \left[\frac{\text{keV}}{T} \right]^3 \\ &\simeq 1.8 \times 10^{-8} \text{ s} \left[\frac{100 \text{ mb}}{\langle\sigma_{\text{had}}v\rangle} \right] \left[\frac{6 \times 10^{-10}}{\eta} \right] \left[\frac{t}{1 \text{ s}} \right]^{3/2}, \end{aligned} \quad (22)$$

where $\langle\sigma_{\text{had}}v\rangle$ is the thermally averaged strong interaction cross section. For the decay times of greatest interest here, $10^4 \text{ s} \lesssim \tau \lesssim 10^8 \text{ s}$, this interaction time is long compared to the typical meson (π, K) lifetime, $(E_{\text{Meson}}/m_{\text{Meson}}) \times 10^{-8} \text{ s}$. The produced mesons thus decay before they interact with background hadrons.

As a result, the hadronic activity from the dominant two-body decay of slepton is negligibly small. The main contributions to hadronic activity therefore come from three-body decays, $\tilde{l} \rightarrow lZ\tilde{G}, \nu_l W\tilde{G}$ with Z or W decaying hadronically, or from four-body decays $\tilde{l} \rightarrow l\gamma^*\tilde{G}$ with $\gamma^* \rightarrow q\bar{q}$. The corresponding Feynman diagrams are shown in Fig. 3. Formulae for the decay amplitudes and decay width calculations are listed in the Appendix.

The hadronic branching fraction is defined as follow:

$$B_{\text{had}} \equiv \frac{\Gamma(\tilde{l} \rightarrow lZ\tilde{G})B_{\text{h}}^Z + \Gamma(\tilde{l} \rightarrow \nu_l W\tilde{G})B_{\text{h}}^W + \Gamma(\tilde{l} \rightarrow l'q\bar{q}\tilde{G})}{\Gamma(\tilde{l} \rightarrow l\tilde{G})}, \quad (23)$$

where $B_{\text{h}}^Z, B_{\text{h}}^W \simeq 0.7$ are the Z and W hadronic branching fractions. For right-handed sleptons, $\Gamma(\tilde{l} \rightarrow \nu_l W\tilde{G}) = 0$, and there are additional suppressions because the Z couplings are smaller than the W couplings. Thus, the hadronic branching fraction of right-handed sleptons is smaller than that of left-handed ones, especially when $m_W < \Delta m < m_Z$.

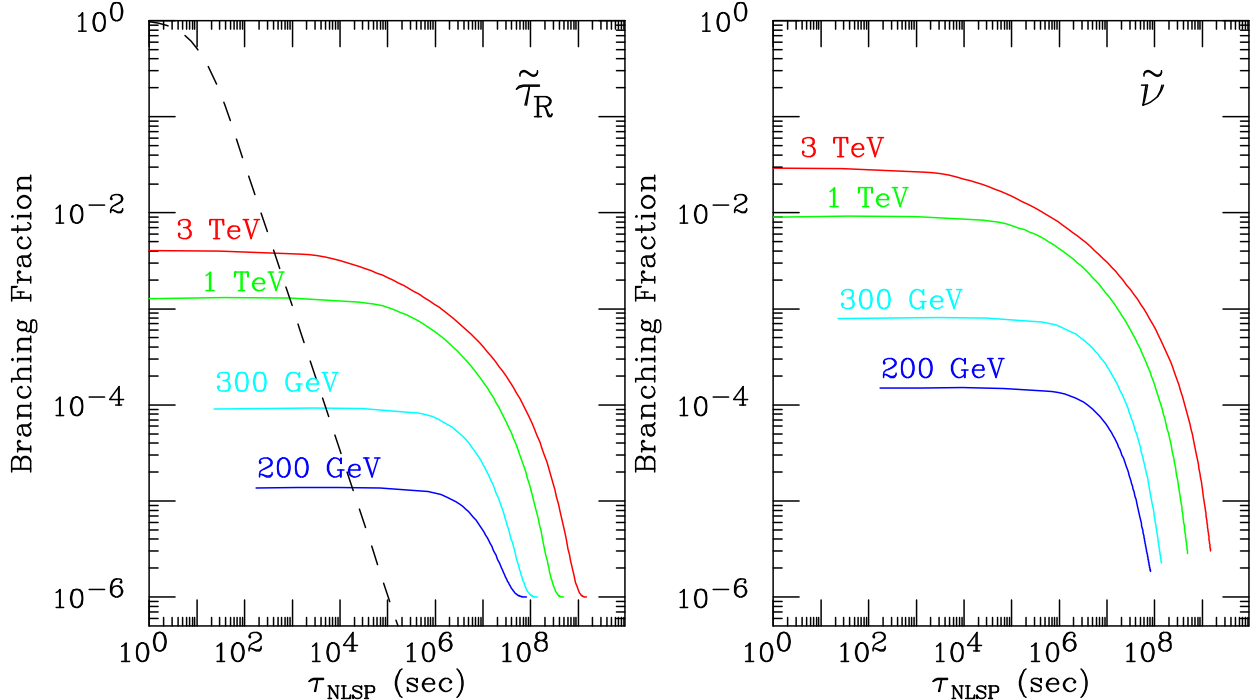


FIG. 4: Hadronic branching fractions for (left) $\tilde{\tau}_R$ NLSPs and (right) $\tilde{\nu}$ NLSPs as functions of the NLSP decay lifetime. Along each curve, the NLSP mass is fixed at the value indicated and the gravitino mass varies. The neutralino/chargino parameters are chosen to be $M_1 = 2m_{\text{NLSP}}$, $M_2 = \mu = 4m_{\text{NLSP}}$, and $\tan\beta = 10$. For the $\tilde{\tau}_R$ case, the dashed line gives the hadronic branching fraction resulting from $\tilde{\tau}_R \rightarrow \tau\tilde{G}$, where the tau decays to a meson, and the meson interacts hadronically before decaying. We take the meson rest lifetime to be 3×10^{-8} s.

For small Δm , the slepton lifetime increases dramatically, since it grows as $(\Delta m)^{-4}$ by Eq. (20). For $\Delta m < m_W$, three-body decay modes are kinematically suppressed and four-body decay through a virtual photon dominates. The branching fraction of four-body decay is roughly expected to be $\mathcal{O}((\alpha/4\pi)^2) \sim \mathcal{O}(10^{-6})$, which sets a lower limit for the hadronic branching fraction. Adjusting this estimation by taking into account details of the kinematics has negligible impact to our results.

For the sneutrino NLSP case, the constraints from bounds on EM energy release are weak, especially at late times $\tau \gtrsim 10^7$ s, as discussed in Sec. III. However, the hadronic energy release is of the same magnitude for sneutrino NLSPs and for left-handed slepton NLSPs. The major hadronic activity comes from three-body decays, $\tilde{\nu} \rightarrow \nu Z\tilde{G}$, $lW\tilde{G}$. The branching fraction for the four-body decay $\tilde{\nu} \rightarrow \nu\gamma^*\tilde{G} \rightarrow \nu q\bar{q}\tilde{G}$ is also similar to the analogous decay in the slepton case, except that diagrams (a) and (b) in Fig. 3 are absent since the neutrino is neutral. Last, we note that in the special case where the Bino and Wino masses are nearly equal, diagram (c) of Fig. 3 is highly suppressed, since the gauge boson V is almost purely Z .

In Fig. 4 we show the hadronic branching fractions for $\tilde{\tau}_R$ and $\tilde{\nu}$ NLSPs for a particular set of values of M_1 , M_2 , μ and $\tan\beta$. Varying these parameters typically does not change our results significantly. The reason is that these parameters only affect the neutralino/chargino appearing in diagram (c) of Fig. 3. The contribution from diagram (c) is negligible if the neutralino/chargino is not degenerate to within about 10% with the sleptons. In addition,

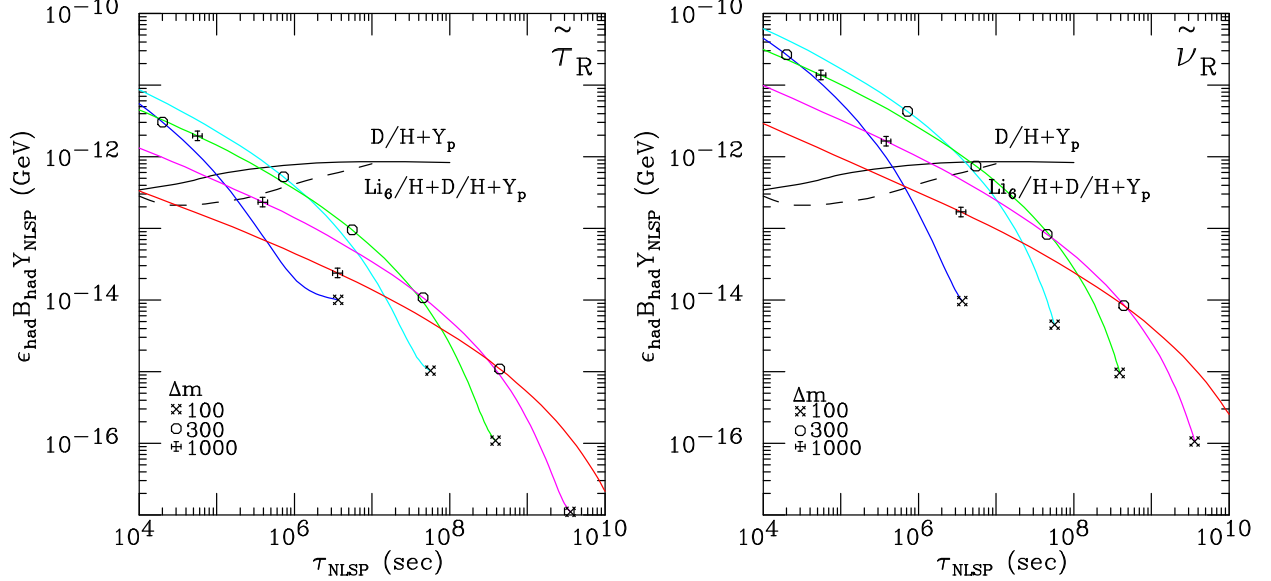


FIG. 5: Hadronic energy releases $\xi_{\text{had}} \equiv \epsilon_{\text{had}} B_{\text{had}} Y_{\text{NLSP}}$ as a function of decay lifetime τ_{NLSP} for (left) $\tilde{\tau}_R$ NLSPs and (right) $\tilde{\nu}$ NLSPs. Along each curve, $m_{\tilde{G}}$ is held fixed and $\Delta m \equiv m_{\text{NLSP}} - m_{\tilde{G}}$ varies. Particular values of Δm are marked by the symbols indicated. The gravitino mass is $m_{\tilde{G}} = 10, 10^2, 10^3, 10^4$ and 10^5 GeV for the curves ordered from left to right by their value at $\Delta m = 100$ GeV. Constraints from BBN [15], with and without ${}^6\text{Li}/\text{H}$, are also shown; regions above the curves are disfavored. We have assumed $\Omega_{\text{SWIMP}} = 0.23$ and $\epsilon_{\text{had}} = \frac{1}{3}(m_{\text{NLSP}} - m_{\tilde{G}})$.

diagram (c) does not interfere with the other diagrams if all couplings are real, which eliminates the possibility of cancelation. Hadronic branching fractions for left-handed sleptons are similar to those shown for sneutrinos. The branching fractions are smaller for the right-handed slepton case for the reasons mentioned above. In both cases, the hadronic branching fractions drop quickly for lifetime $\tau \gtrsim 10^6$ s, which corresponds to small δm . For the $\tilde{\tau}_R$ case, mesons produced in τ decay may, in principle, induce showers before they decay, as discussed above. This contribution to hadronic energy is also shown in Fig. 4. As can be seen, it is important only at early times $\tau \lesssim 10^2 - 10^4$ s and may be safely ignored for the decay times of most interest here.

Note that the hadronic branching fraction of Eq. (23) is defined at the quark level. Hadronization effects are important — for example, as we have shown above, mesons produced in Z and W decays do not contribute to hadronic cascades since they decay before they interact. Such effects have been included in deriving the hadronic BBN constraints that we use [15].

Fig. 5 shows the hadronic energy injection $\xi_{\text{had}} \equiv \epsilon_{\text{had}} B_{\text{had}} Y_{\text{NLSP}}$ as a function of decay lifetime τ_{NLSP} for $\tilde{\tau}_R$ and $\tilde{\nu}$ NLSPs. Along each curve, $m_{\tilde{G}}$ is held fixed and $\Delta m \equiv m_{\text{NLSP}} - m_{\tilde{G}}$ varies. The curves are truncated at $\Delta m = 100$ GeV because for smaller Δm , three-body hadronic decays are highly suppressed, leading to negligible hadronic energy injection. Hadronic BBN constraints from Ref. [15] are also shown, with and without ${}^6\text{Li}$; the regions above the curves are disfavored. It is clear that for larger $m_{\tilde{G}}$, larger values of Δm becomes viable. Constraints are stronger in the $\tilde{\nu}$ case than in the $\tilde{\tau}_R$ case because the hadronic branching fraction is larger for left-handed particles than for right-handed ones. Notice that we have fixed $\Omega_{\text{SWIMP}} = 0.23$ in these plots. The lines could be simply rescaled for other

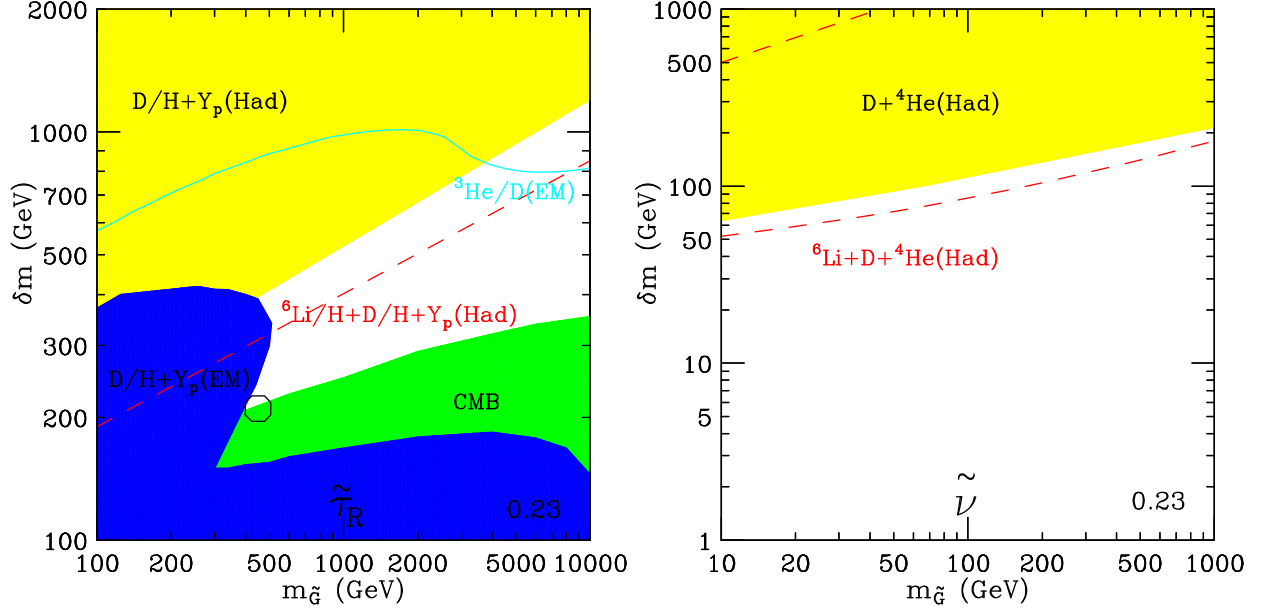


FIG. 6: Allowed and disfavored regions of the $(m_{\tilde{G}}, \delta m)$ plane, where $\delta m \equiv m_{\text{NLSP}} - m_{\tilde{G}} - m_Z$, for (left) $\tilde{\tau}_R$ and (right) $\tilde{\nu}$ NLSPs. The shaded regions are disfavored by CMB, EM BBN, and hadronic BBN constraints, as indicated. The lines correspond to EM constraints from ${}^3\text{He}/\text{D}$ (solid) and hadronic constraints from ${}^6\text{Li}/\text{H}$ (dashed). The circle indicates the best fit region where the ${}^7\text{Li}$ discrepancy is resolved. See text for details. We have assumed $\Omega_{\text{SWIMP}} = 0.23$ and $\epsilon_{\text{had}} = \frac{1}{3}(m_{\text{NLSP}} - m_{\tilde{G}})$. Note that the axes have different scales in the left and right panels.

values of Ω_{SWIMP} since $Y_{\text{NLSP}} \propto \Omega_{\text{SWIMP}}$. We have also adopted the hadronic BBN analysis of Ref. [15]. If updated analyses of the BBN constraints become available, it is straightforward to impose it in these plots to find out the remaining viable parameter regions for $m_{\tilde{G}}$ and Δm .

Fig. 6 shows the allowed and disfavored regions of the $(m_{\tilde{G}}, \delta m)$ plane for the two NLSP cases. The CMB μ distortion constraint, the EM BBN constraint of Ref. [27], and the hadronic BBN constraint of Ref. [15] are included. For the $\tilde{\tau}_R$ case, the CMB constraint excludes a region with $\delta m \lesssim 150 - 300$ GeV. EM BBN constraints from $\text{D}/\text{H} + Y_p$ disfavor regions of δm below 400 GeV for $m_{\tilde{G}} \lesssim 500$ GeV and δm below about 200 GeV for larger $m_{\tilde{G}}$. Hadronic BBN constraints from $\text{D}/\text{H} + Y_p$ disfavor the part of the parameter space with large δm where the slepton decays relatively early. Note that the hadronic constraint is extremely important — it disfavors a large and natural part of parameter space that would otherwise be allowed.

Even after all of these constraints, however, the unshaded area in the region $m_{\tilde{G}} \gtrsim 200$ GeV and $200 \text{ GeV} \lesssim \delta m \lesssim 1500$ GeV still remains viable. The $\tilde{\tau}_R$ mass must be above 500 GeV, but this is within reach of the LHC. The “best fit” point where the ${}^7\text{Li}$ discrepancy is fixed by EM energy release from late slepton decays is indicated by a circle at $(m_{\tilde{G}}, \delta m) \approx (450 \text{ GeV}, 200 \text{ GeV})$. Note that it also remains viable, even given the strong hadronic BBN constraints.

We also indicate the region that is disfavored by the less solid, but stronger, constraints from ${}^3\text{He}/\text{D}$ and ${}^6\text{Li}/\text{H}$. The ${}^3\text{He}/\text{D}$ constraint excludes parameter space below the solid line. The allowed region would then be pushed up to larger $m_{\tilde{G}} \gtrsim 3500$ GeV and larger

$\delta m \gtrsim 800$ GeV. Such a heavy stau NLSP is beyond the reach of the next generation hadron colliders. On the other hand, taking the ${}^6\text{Li}/\text{H}$ constraint literally would exclude parameter space above the dashed line. Taking both constraints literally and combining them would exclude most of the region of parameter space shown. Clearly, a more firm understanding of BBN will have important consequences for the stau NLSP superWIMP scenario.

We have assumed $\Omega_{\text{SWIMP}} = 0.23$; of course, the allowed parameter space would be enlarged if $\Omega_{\text{SWIMP}} < 0.23$. We have also taken $\epsilon_{\text{had}} = \frac{1}{3}(m_{\text{NLSP}} - m_{\tilde{G}})$ in our analysis; the allowed region could shift if there are significant corrections to this relation.

The sneutrino NLSP case is also shown in Fig. 6. Hadronic BBN constraints from the D/H and Y_p abundances only disfavor $\delta m \gtrsim 100$ GeV. Even including the stronger but more speculative ${}^6\text{Li}/\text{H}$ constraint, there is still a large region of $(m_{\tilde{G}}, \delta m)$ that is allowed. The origin of this result is that at $\tau \gtrsim 10^8$ s, the sneutrino NLSP is completely free of hadronic BBN constraints. We have again assumed $\Omega_{\text{SWIMP}} = 0.23$. To get this relic density from a sneutrino thermal relic density, one would typically require sneutrino masses above 500 GeV. However, even assuming a thermal relic abundance, if the superWIMP component is only part of the present dark matter, smaller sneutrino masses are allowed.

For right-handed selectron and smuon NLSPs, the results will be similar to the right-handed stau NLSP case. The EM constraints are slightly stronger, since all the released energy induces EM cascades. For left-handed slepton NLSPs, the region of $(m_{\tilde{G}}, \delta m)$ that is disfavored by hadronic injection is similar to the region disfavored for the sneutrino NLSP. In addition, however, there are EM BBN constraints that are similar to those for right-handed slepton NLSPs.

V. CONCLUSIONS

In this paper, we explored the possibility of superWIMPs as candidates for dark matter. Examples of superWIMPs are the gravitino in supersymmetric models and the lightest Kaluza-Klein graviton in universal extra dimension models. SuperWIMPs obtain their relic density through late decays: $\text{WIMP} \rightarrow \text{superWIMP} + \text{SM particles}$. The decay usually occurs between 10^4 s and 10^8 s, which has important cosmological implications. Such late decays release EM and hadronic energy into the Universe, which may affect BBN predictions for the primordial abundance of the light elements. The constraints on EM injection have been studied in detail in Ref. [2]. In this paper, we have analyzed the hadronic BBN constraints. We have taken the lightest gravitino as a concrete example of a superWIMP and have focused on slepton and sneutrino NLSPs as the most promising WIMP candidates.

We have determined the hadronic energy release by calculating three-body decay widths in detail. For the cases of $\tilde{\tau}_R$ and $\tilde{\nu}$ NLSPs, the hadronic decay branching fraction is below the level of 10^{-3} when $m_{\tilde{\tau}_R} \lesssim 1$ TeV and $m_{\tilde{\nu}} \lesssim 300$ GeV, respectively, or when the decay lifetime is $\tau \gtrsim 10^6$ s. We identified the allowed and disfavored regions of the $(m_{\tilde{G}}, \delta m)$ plane, imposing CMB constraints, EM BBN constraints, and hadronic BBN constraints. For the sneutrino NLSP case, $\delta m \lesssim 60 - 200$ GeV is allowed for a large range of $m_{\tilde{G}}$. For the stau NLSP, the hadronic constraints are weaker: $\delta m \lesssim 200 - 1200$ GeV. However, additional constraints from CMB and EM energy injection apply. Combining all the constraints for the right-handed stau NLSP, the allowed window is $300 \text{ GeV} \lesssim m_{\tilde{G}} \lesssim 1 \text{ TeV}$, $200 \text{ GeV} \lesssim \delta m \lesssim 1200 \text{ GeV}$, corresponding to $m_{\tilde{\tau}_R} \gtrsim 500$ GeV. We have assumed $\Omega_{\text{SWIMP}} = 0.23$ in our analysis. The constraints would be relaxed if superWIMPs are only part of the present dark matter. In addition, there are still ambiguities in the BBN constraints if the decay time lies

in the region where EM and hadronic effects are comparable. In particular, as we discussed, their effects on D might cancel, and the allowed parameter space could be enlarged. Progress in firming up BBN constraints in this region, and for other elements, such as ${}^3\text{He}$ and ${}^6\text{Li}$ may have crucial implications for the superWIMP dark matter scenario.

Although the superWIMP itself would escape all direct and indirect dark matter searches, the slepton/sneutrino NLSP will have rich implications for collider phenomenology. Such metastable sleptons will not decay inside the detector, resulting in signals of highly ionizing tracks for sleptons and missing energy signals for sneutrinos. Discussion of the collider phenomenology, combined with thermal relic density calculations for the NLSP in supergravity models will be presented in Ref. [18].

Although we have focused on the SUSY scenario in this paper, superWIMPs could in general be any gravitationally interacting particle that obtains its relic density through the late decay of a WIMP. The discussion and results for late decay of a leptonic WIMP in other models will be qualitatively similar to the discussion and results presented here. This scenario also suggests that a particle that appears to play the role of dark matter at late times, even after BBN, could very well be different from the particle that constitutes dark matter now. The very late decay of “would be” dark matter particles may have important cosmological implications, for example, affecting small scale structure. This feature may provide qualitatively new possibilities for explaining puzzling cosmological observations [38, 39].

We have assumed R -parity conservation in our discussion. In the case of R -parity violation (RPV), the gravitino could still constitute dark matter as long as its decay lifetime is comparable to or longer than the age of Universe [40, 41]. Gravitino dark matter in an RPV scenario could be distinguished from the superWIMP scenario by both cosmological observations and collider experiments. For example, the decay of even a tiny amount of gravitino dark matter into SM particles in an RPV scenario could be seen in the diffuse photon flux. In addition, if the RPV is not extremely small, the collider signatures could be different from those in the superWIMP scenario. Further work is needed to study how to distinguish these two scenarios.

Acknowledgments

We are grateful to M. Fujii, K. Kohri, T. Moroi, and A. Rajaraman for helpful conversations. The work of JLF was supported in part by National Science Foundation CAREER Grant PHY-0239817, and in part by the Alfred P. Sloan Foundation.

APPENDIX: WIDTHS FOR THREE-BODY SLEPTON DECAYS

1. Interactions

The gravitino-gaugino-gauge boson interaction is

$$\mathcal{L} = -\frac{i}{8M_*} \bar{\psi}_\mu [\gamma^\nu, \gamma^\rho] \gamma^\mu \lambda F_{\nu\rho} , \quad (\text{A.1})$$

where $M_* = \sqrt{2}M_4 = 2.4 \times 10^{18}$ GeV is the reduced Planck mass, and $\psi_\mu \equiv \psi_\mu(x)$ denotes the gravitino field at spacetime point x . The gravitino-slepton-lepton interaction is

$$\mathcal{L} = -\frac{1}{\sqrt{2}M_*} \partial_\nu \tilde{l} \bar{l}_h \gamma^\mu \gamma^\nu \psi_\mu, \quad (\text{A.2})$$

where subscript $h = L, R$ denotes the lepton chirality. In addition, there are gravitino-slepton-lepton-gauge boson interactions:

$$\mathcal{L} = \frac{ieg_V^{lh}}{\sqrt{2}M_*} A_\nu \tilde{l} \bar{l}_h \gamma^\mu \gamma^\nu \psi_\mu. \quad (\text{A.3})$$

Here g_V^{lh} is the gauge coupling coefficient, which is given explicitly below.

Since gravitinos are Majorana particles,

$$\psi_\mu^c \equiv C \bar{\psi}_\mu^T = \psi_\mu. \quad (\text{A.4})$$

The gravitino spin sum (with four momentum p_μ) is

$$\begin{aligned} \sum_h \tilde{G}_\mu^h(p) \overline{\tilde{G}_\nu^h(p)} &= -(\gamma \cdot p + m_{\tilde{G}}) \left(g_{\mu\nu} - \frac{p_\mu p_\nu}{m_{\tilde{G}}^2} \right) \\ &\quad - \frac{1}{3} \left(\gamma_\mu + \frac{p_\mu}{m_{\tilde{G}}} \right) (\gamma \cdot p - m_{\tilde{G}}) \left(\gamma_\nu + \frac{p_\nu}{m_{\tilde{G}}} \right). \end{aligned} \quad (\text{A.5})$$

2. Matrix Amplitudes

Here we present the matrix amplitudes for the three-body decays $\tilde{l} \rightarrow l' V \tilde{G}$, where l' is the SM partner of \tilde{l} or its weak isospin partner, and $V = Z$ or W . The Feynman diagrams are shown in Fig. 3.

We define the following ten operators:

$$\mathcal{O}_1 = \bar{l}_h' p_{l'} \cdot \tilde{G}^c p_{l'} \cdot \epsilon^* \quad (\text{A.6})$$

$$\mathcal{O}_2 = \bar{l}_h' p_l \cdot \tilde{G}^c p_{l'} \cdot \epsilon^* \quad (\text{A.7})$$

$$\mathcal{O}_3 = \bar{l}_h' p_{\tilde{G}} \cdot \tilde{G}^c p_{l'} \cdot \epsilon^* \quad (\text{A.8})$$

$$\mathcal{O}_4 = i \bar{l}_h' \gamma \cdot \epsilon^* p_V \cdot \tilde{G}^c \quad (\text{A.9})$$

$$\mathcal{O}_5 = \bar{l}_h' \gamma \cdot p_V \gamma \cdot \epsilon^* p_{l'} \cdot \tilde{G}^c \quad (\text{A.10})$$

$$\mathcal{O}_6 = i \bar{l}_h' \gamma \cdot p_V \gamma \cdot \epsilon^* p_V \cdot \tilde{G}^c \quad (\text{A.11})$$

$$\mathcal{O}_7 = i \bar{l}_h' \gamma \cdot p_{\tilde{G}} \gamma \cdot \epsilon^* p_V \cdot \tilde{G}^c \quad (\text{A.12})$$

$$\mathcal{O}_8 = i \bar{l}_h' \epsilon^* \cdot \tilde{G}^c \quad (\text{A.13})$$

$$\mathcal{O}_9 = i \bar{l}_h' \gamma \cdot p_V \epsilon^* \cdot \tilde{G}^c \quad (\text{A.14})$$

$$\mathcal{O}_{10} = i \bar{l}_h' \gamma \cdot p_{\tilde{G}} \gamma \cdot p_V \epsilon^* \cdot \tilde{G}^c, \quad (\text{A.15})$$

where ϵ_μ^* is the polarization of gauge boson V . Notice that for an on-shell gravitino in the final state, $\mathcal{O}_3 = 0$ by using the gravitino equation of motion.

In terms of these operators, the matrix elements for three-body slepton decay [diagrams (a)–(d) in Fig. 3] are

$$\mathcal{M}_V^a = \frac{eg_V^{lh}}{\sqrt{2}M_* m_{23}^2} (2\mathcal{O}_1 - \mathcal{O}_5) \quad (\text{A.16})$$

$$\mathcal{M}_V^b = \frac{eg_V^{lh}}{\sqrt{2}M_* m_G^2 + m_V^2 - m_{13}^2 - m_{23}^2} (\mathcal{O}_2 + \mathcal{O}_3) \quad (\text{A.17})$$

$$\mathcal{M}_V^c = \sum_i \frac{eg_{\chi_i}^{lh} g_{\chi_i V}^h}{4M_*} \frac{1}{m_{13}^2 - m_{\chi_i}^2} [m_{\chi_i} (\mathcal{O}_4 - \mathcal{O}_9) - 4(\mathcal{O}_6 + \mathcal{O}_7 - \mathcal{O}_{10}) + m_V^2 \mathcal{O}_8] \quad (\text{A.18})$$

$$\mathcal{M}_V^d = i \frac{\sqrt{2}eg_V^{lh}}{M_*} \mathcal{O}_8, \quad (\text{A.19})$$

where χ_i denotes a neutralino or chargino, the couplings g_V^{lh} , $g_{\chi_i}^{lh}$, and $g_{\chi_i V}$ are given below for each decay process, and

$$m_{12}^2 = (p_{\tilde{G}} + p_V)^2, \quad m_{13}^2 = (p_{\tilde{G}} + p_V)^2, \quad m_{23}^2 = (p_V + p_V)^2. \quad (\text{A.20})$$

Notice that $m_{12}^2 + m_{13}^2 + m_{23}^2 = m_i^2 + m_G^2 + m_Z^2$. Given this relation, the four-momentum scalar products that appear below in the expressions for squared matrix elements can be expressed in terms of m_{12}^2 , m_{13}^2 and m_{23}^2 .

For each specific decay, the couplings in Eqs. (A.16)–(A.19) should be replaced according to the following rules:

- $\tilde{l}_L \rightarrow lZ\tilde{G}$

$$h \rightarrow L, \quad V \rightarrow Z \quad (\text{A.21})$$

$$g_V^{lh} \rightarrow g_Z^{lL} = \frac{1}{\sin\theta_W \cos\theta_W} \left(\frac{1}{2} - \sin^2\theta_W \right) \quad (\text{A.22})$$

$$g_{\chi_i}^{lh} \rightarrow g_{\chi_i^0}^{lL} = \frac{1}{\sqrt{2} \sin\theta_W \cos\theta_W} (N_{i2}^* \cos\theta_W + N_{i1}^* \sin\theta_W) \quad (\text{A.23})$$

$$g_{\chi_i V}^h \rightarrow g_{\chi_i Z}^L = N_{i1}^* (-\sin\theta_W) + N_{i2}^* (\cos\theta_W) \quad (\text{A.24})$$

- $\tilde{l}_L \rightarrow \nu W\tilde{G}$ and $\tilde{\nu}_L \rightarrow lW\tilde{G}$

$$h \rightarrow L, \quad V \rightarrow W \quad (\text{A.25})$$

$$g_V^{lh} \rightarrow g_W^{lL} = -\frac{1}{\sqrt{2} \sin\theta_W} \quad (\text{A.26})$$

$$g_{\chi_i}^{lh} \rightarrow g_{\chi_i^-}^{lL} = \frac{1}{\sqrt{2} \sin\theta_W} V_{i1}^* \quad (\text{A.27})$$

$$g_{\chi_i V}^h \rightarrow g_{\chi_i W}^L = V_{i1}^* \quad (\text{A.28})$$

- $\tilde{l}_R \rightarrow lZ\tilde{G}$

$$h \rightarrow R, \quad V \rightarrow Z \quad (\text{A.29})$$

$$g_V^{lh} \rightarrow g_Z^{lR} = \frac{1}{\sin\theta_W \cos\theta_W} (-\sin^2\theta_W) \quad (\text{A.30})$$

$$g_{\chi_i}^{lh} \rightarrow g_{\chi_i^0}^{lR} = -\frac{\sqrt{2}}{\cos\theta_W} N_{i1} \quad (\text{A.31})$$

$$g_{\chi_i V}^h \rightarrow g_{\chi_i Z}^R = N_{i1} (-\sin\theta_W) + N_{i2} (\cos\theta_W) \quad (\text{A.32})$$

- $\tilde{\nu}_L \rightarrow \nu Z \tilde{G}$

$$h \rightarrow L, \quad V \rightarrow Z \quad (\text{A.33})$$

$$g_V^{lh} \rightarrow g_Z^{lL} = \frac{1}{\sin \theta_W \cos \theta_W} \left(-\frac{1}{2} \right) \quad (\text{A.34})$$

$$g_{\chi_i}^{lh} \rightarrow g_{\chi_i}^{lL} = \frac{1}{\sqrt{2} \sin \theta_W \cos \theta_W} (N_{i2}^* \cos \theta_W + N_{i1}^* \sin \theta_W) \quad (\text{A.35})$$

$$g_{\chi_i V}^h \rightarrow g_{\chi_i Z}^L = N_{i1}^* (-\sin \theta_W) + N_{i2}^* (\cos \theta_W) \quad (\text{A.36})$$

In these expressions, V and N are matrices that diagonalize the chargino and neutralino mass matrices, following the conventions of Ref. [42].

3. Squared Matrix Elements

The differential decay width is

$$d\Gamma = \frac{1}{(2\pi)^3} \frac{1}{32m_{\tilde{l}}^3} |\mathcal{M}|^2 dm_{13}^2 dm_{23}^2, \quad (\text{A.37})$$

where $\mathcal{M} = \mathcal{M}_V^a + \mathcal{M}_V^b + \mathcal{M}_V^c + \mathcal{M}_V^d$.

The sum of the matrix elements can be written as

$$\mathcal{M}(\tilde{l}_h \rightarrow l' V \tilde{G}) = \mathcal{M}_V^a + \mathcal{M}_V^b + \mathcal{M}_V^c + \mathcal{M}_V^d = \sum_{i=1\dots 10} \mathcal{M}_i \mathcal{O}_i, \quad (\text{A.38})$$

where the \mathcal{M}_i can be read off from Eqs. (A.16)–(A.19) above. The squared matrix element is

$$\begin{aligned} |\mathcal{M}(\tilde{l}_h \rightarrow l' V \tilde{G})|^2 &= \sum_{i=1\dots 10} |\mathcal{M}_i|^2 \mathcal{O}_{i,i} \\ &+ \sum_{i,j=1\dots 10}^{i<j} \Re(\mathcal{M}_i \mathcal{M}_j^*) \mathcal{O}_{i,j}^{\text{re}} + \sum_{i,j=1\dots 10}^{i<j} \Im(\mathcal{M}_i \mathcal{M}_j^*) \mathcal{O}_{i,j}^{\text{im}}. \end{aligned} \quad (\text{A.39})$$

In our calculations, we chose the convention that the diagonalizing matrices V and N are real. All couplings appearing in Eq. (A.16)–(A.19) are therefore real. Thus, all the \mathcal{M}_i are real except for \mathcal{M}_8 , which has both real and imaginary components. The only non-zero contributions to the last term in Eq. (A.39) come from $\Im(\mathcal{M}_i \mathcal{M}_8^*)$ ($i < 8$) and $\Im(\mathcal{M}_8 \mathcal{M}_j^*)$ ($j > 8$). Expressions for $\mathcal{O}_{i,i}$, $\mathcal{O}_{i,j}^{\text{re}}$, $\mathcal{O}_{i,8}^{\text{im}}$ ($i < 8$) and $\mathcal{O}_{8,j}^{\text{im}}$ ($j > 8$) are:

$$\begin{aligned} \mathcal{O}_{1,1} &= -\frac{4}{3m_{\tilde{G}}^2 m_V^2} \left[m_{\tilde{G}}^2 m_{\tilde{l}}^2 - (p_{\tilde{G}} \cdot p_{\tilde{l}})^2 \right] \left[m_{\tilde{G}}^2 - p_{\tilde{G}} \cdot p_{\tilde{l}} + p_{\tilde{G}} \cdot p_V \right] \\ &\times \left[m_{\tilde{G}}^2 m_V^2 + m_{\tilde{l}}^2 m_V^2 - 2m_V^2 p_{\tilde{G}} \cdot p_{\tilde{l}} - (p_{\tilde{G}} \cdot p_V)^2 + 2p_{\tilde{G}} \cdot p_V p_{\tilde{l}} \cdot p_V - (p_{\tilde{l}} \cdot p_V)^2 \right] \end{aligned} \quad (\text{A.40})$$

$$\begin{aligned} \mathcal{O}_{2,2} &= -\frac{4}{3m_{\tilde{G}}^2 m_V^2} \left[m_{\tilde{G}}^2 - p_{\tilde{G}} \cdot p_{\tilde{l}} + p_{\tilde{G}} \cdot p_V \right] \left[m_{\tilde{l}}^2 m_V^2 - (p_{\tilde{l}} \cdot p_V)^2 \right] \\ &\times \left[-(p_{\tilde{G}} \cdot p_{\tilde{l}})^2 + 2p_{\tilde{G}} \cdot p_{\tilde{l}} p_{\tilde{G}} \cdot p_V - (p_{\tilde{G}} \cdot p_V)^2 + m_{\tilde{G}}^2 (m_{\tilde{l}}^2 + m_V^2 - 2p_{\tilde{l}} \cdot p_V) \right] \end{aligned} \quad (\text{A.41})$$

$$\mathcal{O}_{3,3} = 0 \quad (\text{A.42})$$

$$\begin{aligned}\mathcal{O}_{4,4} &= \frac{4}{3m_G^2 m_V^2} \left[m_G^2 m_V^2 - (p_{\bar{G}} \cdot p_V)^2 \right] \\ &\quad \times \left[m_G^2 m_V^2 - m_V^2 p_{\bar{G}} \cdot p_{\bar{l}} + 2(p_{\bar{G}} \cdot p_V)^2 + p_{\bar{G}} \cdot p_V (3m_V^2 - 2p_{\bar{l}} \cdot p_V) \right]\end{aligned}\quad (\text{A.43})$$

$$\begin{aligned}\mathcal{O}_{5,5} &= -\frac{4}{3m_G^2} \left[m_G^2 m_{\bar{l}}^2 - (p_{\bar{G}} \cdot p_{\bar{l}})^2 \right] \\ &\quad \times \left[m_G^2 m_V^2 - m_V^2 p_{\bar{G}} \cdot p_{\bar{l}} - 4(p_{\bar{G}} \cdot p_V)^2 + p_{\bar{G}} \cdot p_V (-3m_Z^2 + 4p_{\bar{l}} \cdot p_V) \right]\end{aligned}\quad (\text{A.44})$$

$$\begin{aligned}\mathcal{O}_{6,6} &= -\frac{4}{3m_G^2} \left[m_G^2 m_Z^2 - (p_{\bar{G}} \cdot p_V)^2 \right] \\ &\quad \times \left[m_G^2 m_V^2 - m_V^2 p_{\bar{G}} \cdot p_{\bar{l}} - 4(p_{\bar{G}} \cdot p_V)^2 + p_{\bar{G}} \cdot p_V (-3m_V^2 + 4p_{\bar{l}} \cdot p_V) \right]\end{aligned}\quad (\text{A.45})$$

$$\begin{aligned}\mathcal{O}_{7,7} &= \frac{4}{3m_G^2 m_V^2} \left[m_G^2 m_V^2 - (p_{\bar{G}} \cdot p_V)^2 \right] \\ &\quad \left\{ m_G^4 m_V^2 + 2m_G^2 (p_{\bar{G}} \cdot p_V)^2 + 4p_{\bar{G}} \cdot p_V^3 - p_{\bar{G}} \cdot p_{\bar{l}} \left[m_G^2 m_V^2 + 4(p_{\bar{G}} \cdot p_V)^2 \right] \right. \\ &\quad \left. - m_G^2 p_{\bar{G}} \cdot p_V (m_V^2 - 2p_{\bar{l}} \cdot p_V) \right\}\end{aligned}\quad (\text{A.46})$$

$$\mathcal{O}_{8,8} = -\frac{4}{3m_G^2 m_V^2} \left[m_G^2 - p_{\bar{G}} \cdot p_{\bar{l}} + p_{\bar{G}} \cdot p_V \right] \left[2m_G^2 m_V^2 + (p_{\bar{G}} \cdot p_V)^2 \right] \quad (\text{A.47})$$

$$\begin{aligned}\mathcal{O}_{9,9} &= \frac{4}{3m_G^2 m_V^2} \left[2m_G^2 m_V^2 + (p_{\bar{G}} \cdot p_V)^2 \right] \\ &\quad \times \left[m_G^2 m_V^2 - m_V^2 p_{\bar{G}} \cdot p_{\bar{l}} - 2(p_{\bar{G}} \cdot p_V)^2 - p_{\bar{G}} \cdot p_V (m_V^2 - 2p_{\bar{l}} \cdot p_V) \right]\end{aligned}\quad (\text{A.48})$$

$$\begin{aligned}\mathcal{O}_{10,10} &= \frac{4}{3m_G^2 m_V^2} \left[2m_G^2 m_V^2 + (p_{\bar{G}} \cdot p_V)^2 \right] \\ &\quad \left\{ m_G^4 m_V^2 - 2m_G^2 (p_{\bar{G}} \cdot p_V)^2 - 4(p_{\bar{G}} \cdot p_V)^3 \right. \\ &\quad \left. + p_{\bar{G}} \cdot p_{\bar{l}} \left[-m_G^2 m_V^2 + 4(p_{\bar{G}} \cdot p_V)^2 \right] + m_G^2 p_{\bar{G}} \cdot p_V (3m_V^2 - 2p_{\bar{l}} \cdot p_V) \right\}\end{aligned}\quad (\text{A.49})$$

$$\begin{aligned}\mathcal{O}_{1,2}^{\text{re}} &= \frac{8}{3m_G^2 m_V^2} \left[m_G^2 - p_{\bar{G}} \cdot p_{\bar{l}} + p_{\bar{G}} \cdot p_V \right] \\ &\quad \times \left[-(p_{\bar{G}} \cdot p_{\bar{l}})^2 + p_{\bar{G}} \cdot p_{\bar{l}} p_{\bar{G}} \cdot p_V + m_G^2 (m_{\bar{l}}^2 - p_{\bar{l}} \cdot p_V) \right] \\ &\quad \times \left[-m_{\bar{l}}^2 m_V^2 + m_Z^2 p_{\bar{G}} \cdot p_{\bar{l}} - p_{\bar{G}} \cdot p_V p_{\bar{l}} \cdot p_V + (p_{\bar{l}} \cdot p_V)^2 \right]\end{aligned}\quad (\text{A.50})$$

$$\mathcal{O}_{1,3}^{\text{re}} = \mathcal{O}_{1,4}^{\text{re}} = 0 \quad (\text{A.51})$$

$$\begin{aligned}\mathcal{O}_{1,5}^{\text{re}} &= \frac{8}{3m_G^2} \left[m_G^2 m_{\bar{l}}^2 - (p_{\bar{G}} \cdot p_{\bar{l}})^2 \right] \left[-(p_{\bar{G}} \cdot p_V)^2 + m_G^2 (m_V^2 - p_{\bar{l}} \cdot p_V) \right] \\ &\quad + p_{\bar{G}} \cdot p_V (-m_{\bar{l}}^2 + p_{\bar{l}} \cdot p_V) + p_{\bar{G}} \cdot p_{\bar{l}} (-m_V^2 + p_{\bar{G}} \cdot p_V + p_{\bar{l}} \cdot p_V)\end{aligned}\quad (\text{A.52})$$

$$\mathcal{O}_{1,6}^{\text{re}} = \mathcal{O}_{1,7}^{\text{re}} = \mathcal{O}_{1,8}^{\text{re}} = \mathcal{O}_{1,9}^{\text{re}} = \mathcal{O}_{1,10}^{\text{re}} = 0 \quad (\text{A.53})$$

$$\mathcal{O}_{2,3}^{\text{re}} = \mathcal{O}_{2,4}^{\text{re}} = 0 \quad (\text{A.54})$$

$$\begin{aligned}\mathcal{O}_{2,5}^{\text{re}} &= \frac{4}{3m_G^2} \left\{ (p_{\bar{G}} \cdot p_{\bar{l}})^2 \left[m_G^2 m_V^2 + 2(m_{\bar{l}}^2 - m_V^2) p_{\bar{G}} \cdot p_V \right] \right. \\ &\quad + 2(p_{\bar{G}} \cdot p_{\bar{l}})^3 (m_V^2 - p_{\bar{l}} \cdot p_V) - 2p_{\bar{G}} \cdot p_{\bar{l}} \left[(p_{\bar{G}} \cdot p_V)^2 (m_{\bar{l}}^2 - p_{\bar{l}} \cdot p_V) \right. \\ &\quad \left. \left. + m_G^2 (m_{\bar{l}}^2 - p_{\bar{l}} \cdot p_V) (m_V^2 - p_{\bar{l}} \cdot p_V) + m_G^2 p_{\bar{G}} \cdot p_V p_{\bar{l}} \cdot p_V \right] \right\}\end{aligned}$$

$$+m_{\tilde{G}}^2 \left[m_{\tilde{l}}^2 (p_{\tilde{G}} \cdot p_V)^2 - 2p_{\tilde{G}} \cdot p_V (m_{\tilde{l}}^2 - p_{\tilde{l}} \cdot p_V)^2 + m_{\tilde{G}}^2 (-m_{\tilde{l}}^2 m_V^2 + (p_{\tilde{l}} \cdot p_V)^2) \right] \quad (\text{A.55})$$

$$\mathcal{O}_{2,6}^{\text{re}} = \mathcal{O}_{2,7}^{\text{re}} = \mathcal{O}_{2,8}^{\text{re}} = \mathcal{O}_{2,9}^{\text{re}} = \mathcal{O}_{2,10}^{\text{re}} = 0 \quad (\text{A.56})$$

$$\mathcal{O}_{3,4}^{\text{re}} = \mathcal{O}_{3,5}^{\text{re}} = \mathcal{O}_{3,6}^{\text{re}} = \mathcal{O}_{3,7}^{\text{re}} = \mathcal{O}_{3,8}^{\text{re}} = \mathcal{O}_{3,9}^{\text{re}} = \mathcal{O}_{3,10}^{\text{re}} = 0 \quad (\text{A.57})$$

$$\mathcal{O}_{4,5}^{\text{re}} = 0 \quad (\text{A.58})$$

$$\mathcal{O}_{4,6}^{\text{re}} = \frac{8}{m_{\tilde{G}}} \left[m_{\tilde{G}}^2 m_V^2 - (p_{\tilde{G}} \cdot p_V)^2 \right] \left[m_V^2 + p_{\tilde{G}} \cdot p_V - p_{\tilde{l}} \cdot p_V \right] \quad (\text{A.59})$$

$$\mathcal{O}_{4,7}^{\text{re}} = \frac{8}{m_{\tilde{G}}} \left[m_{\tilde{G}}^2 - p_{\tilde{G}} \cdot p_{\tilde{l}} + p_{\tilde{G}} \cdot p_V \right] \left[m_{\tilde{G}}^2 m_V^2 - (p_{\tilde{G}} \cdot p_V)^2 \right] \quad (\text{A.60})$$

$$\mathcal{O}_{4,8}^{\text{re}} = \frac{8}{3m_{\tilde{G}} m_V^2} \left[-m_V^2 (m_{\tilde{G}}^2 - 2p_{\tilde{G}} \cdot p_{\tilde{l}}) p_{\tilde{G}} \cdot p_V + p_{\tilde{G}} \cdot p_V^3 + m_{\tilde{G}}^2 m_V^2 (m_V^2 - p_{\tilde{l}} \cdot p_V) - (p_{\tilde{G}} \cdot p_V)^2 (m_V^2 + p_{\tilde{l}} \cdot p_V) \right] \quad (\text{A.61})$$

$$\mathcal{O}_{4,9}^{\text{re}} = \frac{8}{3m_{\tilde{G}}^2 m_V^2} \left[m_{\tilde{G}}^4 m_V^4 + m_{\tilde{G}}^2 m_V^4 p_{\tilde{G}} \cdot p_V + m_{\tilde{G}}^2 m_V^2 (p_{\tilde{G}} \cdot p_V)^2 - 2(p_{\tilde{G}} \cdot p_V)^4 - m_V^2 p_{\tilde{G}} \cdot p_{\tilde{l}} (m_{\tilde{G}}^2 m_V^2 + (p_{\tilde{G}} \cdot p_V)^2) - (p_{\tilde{G}} \cdot p_V)^3 (m_V^2 - 2p_{\tilde{l}} \cdot p_V) \right] \quad (\text{A.62})$$

$$\mathcal{O}_{4,10}^{\text{re}} = \frac{8}{3m_{\tilde{G}}} \left\{ m_{\tilde{G}}^4 m_V^2 - m_{\tilde{G}}^2 (p_{\tilde{G}} \cdot p_V)^2 - 3p_{\tilde{G}} \cdot p_V^3 + p_{\tilde{G}} \cdot p_{\tilde{l}} [-m_{\tilde{G}}^2 m_V^2 + 3(p_{\tilde{G}} \cdot p_V)^2] + m_{\tilde{G}}^2 p_{\tilde{G}} \cdot p_V (3m_V^2 - 2p_{\tilde{l}} \cdot p_V) \right\} \quad (\text{A.63})$$

$$\mathcal{O}_{5,6}^{\text{re}} = \mathcal{O}_{5,7}^{\text{re}} = \mathcal{O}_{5,8}^{\text{re}} = \mathcal{O}_{5,9}^{\text{re}} = \mathcal{O}_{5,10}^{\text{re}} = 0 \quad (\text{A.64})$$

$$\mathcal{O}_{6,7}^{\text{re}} = \frac{8}{3m_{\tilde{G}}^2} \left[m_{\tilde{G}}^2 m_V^2 - (p_{\tilde{G}} \cdot p_V)^2 \right] \times \left[(3m_{\tilde{G}}^2 - 2p_{\tilde{G}} \cdot p_{\tilde{l}}) p_{\tilde{G}} \cdot p_V + 2(p_{\tilde{G}} \cdot p_V)^2 + m_{\tilde{G}}^2 (m_V^2 - p_{\tilde{l}} \cdot p_V) \right] \quad (\text{A.65})$$

$$\mathcal{O}_{6,8}^{\text{re}} = -\frac{8}{3m_{\tilde{G}}^2} \left[m_{\tilde{G}}^4 m_V^2 - m_{\tilde{G}}^2 (p_{\tilde{G}} \cdot p_V)^2 + (p_{\tilde{G}} \cdot p_V)^3 - p_{\tilde{G}} \cdot p_{\tilde{l}} (m_{\tilde{G}}^2 m_V^2 + (p_{\tilde{G}} \cdot p_V)^2) - m_{\tilde{G}}^2 p_{\tilde{G}} \cdot p_V (m_V^2 - 2p_{\tilde{l}} \cdot p_V) \right] \quad (\text{A.66})$$

$$\mathcal{O}_{6,9}^{\text{re}} = \frac{8}{3m_{\tilde{G}}} \left[m_V^2 (3m_{\tilde{G}}^2 - 2p_{\tilde{G}} \cdot p_{\tilde{l}}) p_{\tilde{G}} \cdot p_V - 3(p_{\tilde{G}} \cdot p_V)^3 - (p_{\tilde{G}} \cdot p_V)^2 (m_V^2 - 3p_{\tilde{l}} \cdot p_V) + m_{\tilde{G}}^2 m_V^2 (m_V^2 - p_{\tilde{l}} \cdot p_V) \right] \quad (\text{A.67})$$

$$\mathcal{O}_{6,10}^{\text{re}} = \frac{8}{3m_{\tilde{G}}^2} \left[m_{\tilde{G}}^4 m_V^2 p_{\tilde{G}} \cdot p_V - (m_{\tilde{G}}^2 - 2p_{\tilde{G}} \cdot p_{\tilde{l}}) (p_{\tilde{G}} \cdot p_V)^3 - 2(p_{\tilde{G}} \cdot p_V)^4 + m_{\tilde{G}}^4 m_V^2 (m_V^2 - p_{\tilde{l}} \cdot p_V) + m_{\tilde{G}}^2 (p_{\tilde{G}} \cdot p_V)^2 (m_V^2 - p_{\tilde{l}} \cdot p_V) \right] \quad (\text{A.68})$$

$$\mathcal{O}_{7,8}^{\text{re}} = \frac{8}{3m_{\tilde{G}}^2 m_V^2} \left[m_{\tilde{G}}^4 m_V^2 p_{\tilde{G}} \cdot p_V - (m_{\tilde{G}}^2 - 2p_{\tilde{G}} \cdot p_{\tilde{l}}) (p_{\tilde{G}} \cdot p_V)^3 - 2(p_{\tilde{G}} \cdot p_V)^4 + m_{\tilde{G}}^4 m_V^2 (m_V^2 - p_{\tilde{l}} \cdot p_V) + m_{\tilde{G}}^2 (p_{\tilde{G}} \cdot p_V)^2 (m_V^2 - p_{\tilde{l}} \cdot p_V) \right] \quad (\text{A.69})$$

$$\mathcal{O}_{7,9}^{\text{re}} = \frac{8}{3m_{\tilde{G}}} \left[m_{\tilde{G}}^4 m_V^2 - m_{\tilde{G}}^2 (p_{\tilde{G}} \cdot p_V)^2 + (p_{\tilde{G}} \cdot p_V)^3 - p_{\tilde{G}} \cdot p_{\tilde{l}} (m_{\tilde{G}}^2 m_V^2 + (p_{\tilde{G}} \cdot p_V)^2) - m_{\tilde{G}}^2 p_{\tilde{G}} \cdot p_V (m_V^2 - 2p_{\tilde{l}} \cdot p_V) \right] \quad (\text{A.70})$$

$$\begin{aligned} \mathcal{O}_{7,10}^{\text{re}} = & \frac{8}{3m_{\tilde{G}}^2 m_V^2} \left\{ m_{\tilde{G}}^6 m_V^4 + m_{\tilde{G}}^4 m_V^4 p_{\tilde{G}} \cdot p_V + m_{\tilde{G}}^4 m_V^2 (p_{\tilde{G}} \cdot p_V)^2 \right. \\ & - 2m_{\tilde{G}}^2 (p_{\tilde{G}} \cdot p_V)^4 - 4(p_{\tilde{G}} \cdot p_V)^5 \\ & - p_{\tilde{G}} \cdot p_{\tilde{l}} \left[m_{\tilde{G}}^4 m_V^4 + m_{\tilde{G}}^2 m_V^2 (p_{\tilde{G}} \cdot p_V)^2 - 4(p_{\tilde{G}} \cdot p_V)^4 \right] \\ & \left. + m_{\tilde{G}}^2 (p_{\tilde{G}} \cdot p_V)^3 (3m_V^2 - 2p_{\tilde{l}} \cdot p_V) \right\} \end{aligned} \quad (\text{A.71})$$

$$\mathcal{O}_{8,9}^{\text{re}} = \frac{8}{3m_{\tilde{G}}^2 m_V^2} \left[2m_{\tilde{G}}^2 m_V^2 + (p_{\tilde{G}} \cdot p_V)^2 \right] \left[m_V^2 + p_{\tilde{G}} \cdot p_V - p_{\tilde{l}} \cdot p_V \right] \quad (\text{A.72})$$

$$\begin{aligned} \mathcal{O}_{8,10}^{\text{re}} = & \frac{8}{3m_{\tilde{G}}^2 m_V^2} \left[2m_{\tilde{G}}^2 m_V^2 + (p_{\tilde{G}} \cdot p_V)^2 \right] \\ & \times \left[- (m_{\tilde{G}}^2 - 2p_{\tilde{G}} \cdot p_{\tilde{l}}) p_{\tilde{G}} \cdot p_V - 2(p_{\tilde{G}} \cdot p_V)^2 + m_{\tilde{G}}^2 (m_V^2 - p_{\tilde{l}} \cdot p_V) \right] \end{aligned} \quad (\text{A.73})$$

$$\mathcal{O}_{9,10}^{\text{re}} = \frac{8}{3m_{\tilde{G}}^2} \left[m_{\tilde{G}}^2 - p_{\tilde{G}} \cdot p_{\tilde{l}} + p_{\tilde{G}} \cdot p_V \right] \left[2m_{\tilde{G}}^2 m_V^2 + (p_{\tilde{G}} \cdot p_V)^2 \right] \quad (\text{A.74})$$

$$\begin{aligned} \mathcal{O}_{1,8}^{\text{im}} = & -\frac{8}{3m_{\tilde{G}}^2 m_V^2} (m_{\tilde{G}}^2 - p_{\tilde{G}} \cdot p_{\tilde{l}} + p_{\tilde{G}} \cdot p_V) \left\{ \left[m_{\tilde{l}}^2 m_V^2 - (p_{\tilde{l}} \cdot p_V)^2 + (p_{\tilde{G}} \cdot p_V)(p_{\tilde{l}} \cdot p_V) \right] m_{\tilde{G}}^2 \right. \\ & \left. - m_V^2 (p_{\tilde{G}} \cdot p_{\tilde{l}})^2 + (p_{\tilde{G}} \cdot p_{\tilde{l}})(p_{\tilde{G}} \cdot p_V)(p_{\tilde{l}} \cdot p_V - p_{\tilde{G}} \cdot p_V) \right\} \end{aligned} \quad (\text{A.75})$$

$$\begin{aligned} \mathcal{O}_{2,8}^{\text{im}} = & -\frac{8}{3m_{\tilde{G}}^2 m_V^2} (m_{\tilde{G}}^2 - p_{\tilde{G}} \cdot p_{\tilde{l}} + p_{\tilde{G}} \cdot p_V) \left[(m_{\tilde{l}}^2 m_V^2 - (p_{\tilde{l}} \cdot p_V)^2) m_{\tilde{G}}^2 - m_V^2 (p_{\tilde{G}} \cdot p_{\tilde{l}})^2 \right. \\ & \left. - (p_{\tilde{G}} \cdot p_V)^2 p_{\tilde{l}} \cdot p_V + (p_{\tilde{G}} \cdot p_{\tilde{l}})(p_{\tilde{G}} \cdot p_V)(m_V^2 + p_{\tilde{l}} \cdot p_V) \right] \end{aligned} \quad (\text{A.76})$$

$$\mathcal{O}_{3,8}^{\text{im}} = \mathcal{O}_{4,8}^{\text{im}} = 0 \quad (\text{A.77})$$

$$\begin{aligned} \mathcal{O}_{5,8}^{\text{im}} = & \frac{8}{3m_{\tilde{G}}^2} \left\{ (p_{\tilde{G}} \cdot p_{\tilde{l}} - m_{\tilde{G}}^2) p_{\tilde{l}} \cdot p_V m_{\tilde{G}}^2 - p_{\tilde{G}} \cdot p_{\tilde{l}} (p_{\tilde{G}} \cdot p_V)^2 \right. \\ & \left. + p_{\tilde{G}} \cdot p_V \left[p_{\tilde{G}} \cdot p_{\tilde{l}} m_{\tilde{G}}^2 + (p_{\tilde{l}} \cdot p_V - 2m_{\tilde{l}}^2) m_{\tilde{G}}^2 + (p_{\tilde{G}} \cdot p_{\tilde{l}})^2 \right] \right\} \end{aligned} \quad (\text{A.78})$$

$$\mathcal{O}_{6,8}^{\text{im}} = \mathcal{O}_{7,8}^{\text{im}} = \mathcal{O}_{8,9}^{\text{im}} = \mathcal{O}_{8,10}^{\text{im}} = 0. \quad (\text{A.79})$$

-
- [1] J. L. Feng, A. Rajaraman and F. Takayama, Phys. Rev. Lett. **91**, 011302 (2003) [hep-ph/0302215].
- [2] J. L. Feng, A. Rajaraman and F. Takayama, Phys. Rev. D **68**, 063504 (2003) [hep-ph/0306024].
- [3] J. R. Ellis, D. V. Nanopoulos and S. Sarkar, Nucl. Phys. B **259**, 175 (1985).
- [4] M. Bolz, W. Buchmuller and M. Plumacher, Phys. Lett. B **443**, 209 (1998) [hep-ph/9809381].
- [5] M. Bolz, A. Brandenburg and W. Buchmuller, Nucl. Phys. B **606**, 518 (2001) [hep-ph/0012052].
- [6] J. R. Ellis, K. A. Olive, Y. Santoso and V. Spanos, hep-ph/0312262.
- [7] J. L. Feng, A. Rajaraman and F. Takayama, Phys. Rev. D **68**, 085018 (2003) [hep-ph/0307375].
- [8] SuperWIMP dark matter shares some characteristics with axino dark matter. See L. Covi, J. E. Kim and L. Roszkowski, Phys. Rev. Lett. **82**, 4180 (1999) [hep-ph/9905212]; L. Covi, H. B. Kim, J. E. Kim and L. Roszkowski, JHEP **0105**, 033 (2001) [hep-ph/0101009].
- [9] H. Pagels and J. R. Primack, Phys. Rev. Lett. **48**, 223 (1982).
- [10] T. Moroi, H. Murayama and M. Yamaguchi, Phys. Lett. B **303**, 289 (1993).

- [11] M. H. Reno and D. Seckel, Phys. Rev. D **37**, 3441 (1988).
- [12] K. Kohri, Phys. Rev. D **64**, 043515 (2001) [astro-ph/0103411].
- [13] S. Dimopoulos, R. Esmailzadeh, L. J. Hall and G. D. Starkman, Astrophys. J. **330**, 545 (1988).
- [14] S. Dimopoulos, R. Esmailzadeh, L. J. Hall and G. D. Starkman, Nucl. Phys. B **311**, 699 (1989).
- [15] M. Kawasaki, K. Kohri and T. Moroi, astro-ph/0402490.
- [16] W. Buchmuller, K. Hamaguchi and M. Ratz, Phys. Lett. B **574**, 156 (2003) [hep-ph/0307181].
- [17] E. W. Kolb, A. Notari and A. Riotto, Phys. Rev. D **68**, 123505 (2003) [hep-ph/0307241].
- [18] J. L. Feng, S. Su and F. Takayama, in preparation.
- [19] D. N. Spergel *et al.*, Astrophys. J. Suppl. **148**, 175 (2003) [astro-ph/0302209].
- [20] S. Burles, K. M. Nollett and M. S. Turner, Astrophys. J. **552**, L1 (2001) [astro-ph/0010171].
- [21] D. Kirkman, D. Tytler, N. Suzuki, J. M. O'Meara and D. Lubin, Astrophys. J. Suppl. **149**, 1 (2003) [astro-ph/0302006].
- [22] K. A. Olive, E. Skillman and G. Steigman, Astrophys. J. **483**, 788 (1997) [astro-ph/9611166].
- [23] Y. I. Izotov and T. X. Thuan, Astrophys. J. **500**, 188 (1998).
- [24] J. A. Thorburn, Astrophys. J. **421**, 318 (1994).
- [25] P. Bonifacio and P. Molaro, MNRAS, **285**, 847 (1997).
- [26] S. G. Ryan, T. C. Beers, K. A. Olive, B. D. Fields and J. E. Norris, Astrophys. J. Lett. **530**, L57 (2000) [astro-ph/9905211].
- [27] R. H. Cyburt, J. R. Ellis, B. D. Fields and K. A. Olive, Phys. Rev. D **67**, 103521 (2003) [astro-ph/0211258].
- [28] M. Kawasaki and T. Moroi, Astrophys. J. **452**, 506 (1995) [astro-ph/9412055].
- [29] K. Kohri, private communication.
- [30] T. M. Bania, R. T. Rood and D. S. Balser, Nature **415**, 54 (2002).
- [31] E. Vangioni-Flam, K. A. Olive, B. D. Fields and M. Casse, Astrophys. J. **585**, 611 (2003) [astro-ph/0207583].
- [32] L. Brown and D. N. Schramm, Astrophys. J. **329**, L103 (1988).
- [33] K. Jedamzik, Phys. Rev. Lett. **84**, 3248 (2000) [astro-ph/9909445].
- [34] P. E. Nissen, D. L. Lambert, F. Primas and V. V. Smith, astro-ph/9906306.
- [35] K. Jedamzik, astro-ph/0402344.
- [36] M. Kawasaki and T. Moroi, Phys. Lett. B **346**, 27 (1995) [hep-ph/9408321].
- [37] J. A. Frieman and G. F. Giudice, Phys. Lett. B **224**, 125 (1989).
- [38] X. Chen and M. Kamionkowski, astro-ph/0310473.
- [39] K. Sigurdson and M. Kamionkowski, astro-ph/0311486.
- [40] F. Takayama and M. Yamaguchi, Phys. Lett. B **485**, 388 (2000) [hep-ph/0005214].
- [41] G. Moreau and M. Chemtob, Phys. Rev. D **65**, 024033 (2002) [hep-ph/0107286].
- [42] H. E. Haber and G. L. Kane, Phys. Rept. **117**, 75 (1985).